ISSN 0036-0244, Russian Journal of Physical Chemistry A, 2022, Vol. 96, No. 7, pp. 1474–1483. © Pleiades Publishing, Ltd., 2022.

CHEMICAL THERMODYNAMICS AND THERMOCHEMISTRY

# Thermodynamic Study of Assembling ↔ Disassembling of Microtubules via the Monte Carlo Simulation

**Farnoush Naghsh[a] and Majid Monajjemi[b,*]**

[a] *Department of Chemistry, Science and Research Branch, Islamic Azad University, Tehran, Iran*

[b] *Department of Chemical engineering, Central Tehran Branch, Islamic Azad University, Tehran, Iran*

** e-mail: m_monajjemi@srbiau.ac.ir, maj.monajjemi@iauctb.ac.ir*

Received June 7, 2021; revised October 30, 2021; accepted December 27, 2021

**Abstract**—Microtubules are demonstrated as straight macromolecules including the linear chains of tubulin subunits in the length. It's important to know the functions inside microtubule growth and the control of microtubule processes. An important item that determines the status of a microtubule, whether it is growing or shrinking, is the length of the GTP tubulin microtubule cap in view point of thermodynamic properties. Monte Carlo simulation has been applied to study dynamic instability of the microtubule length. In this model, one-dimensional microtubule is fixed at one of the two and is simulated while the opposite end is allowed for growing in random situation. By a Monte Carlo model of the assembly and disassembly of microtubules, the thermodynamic parameters helped us to explain suitable mechanism and also we take into account the contribution of water to the entropy of the microtubule systems. We compared the result of the model from published experimental data using the GTP tubulin dimer attachment rate and the lateral and longitudinal binding energies of GTP and GDP tubulin dimers at both ends. By this study at each step, one tubulin has been added to the length for growing microtubule length. Computationally, this can be done through generating a uniform random number between 0 and 1. It has been calculated a correct dimension around $10^{-6}$ m of microtubules length including around 1650 tubulin dimers. Microtubule growth rate is related to the soluble tubulin dimer concentration and for all results shown here, simulation of any single condition was run 5–10 times. For each simulation it has been recorded values number, average length and free tubulin concentration.

**Keywords:** tubulin, microtubules, Monte Carlo simulation, thermodynamic law

**DOI:** 10.1134/S0036024422070111

## INTRODUCTION

In past two decades (2005 up to now), a few novel properties have been discovered about the mechanism reaction of stathmin with microtubules (MTs) by researchers [1–10]. The stathmin family proteins carry out a major function in regulating rapid microtubule remodeling of the cytoskeleton and also increase microtubule turnover in response to the cell's needs such as extracellular signals [1]. One molecule stathmin interacts with two subunits tubulins "αβ-tubulin" dimers" for building a tight ternary complex (is known as $T_2S$ complex) which decreases microtubule destabilizing activity near microtubule polymer [2]. One of the important stathmin category proteins is $RB_3$ which shares (88%) with other members the stathmin-like domain (SLD) through translated amino-acid identity with that of XB3 [2, 3]. Since stathmin is a disordered protein and their activities are down-regulated by multiple phosphorylations, it becomes non-polymerizable in complex of the $T_2S$ tubulin [4]. Since the stathmin is a soluble cytoplasmic protein, is used in regulating rapid microtubule remaking of the cytoskeleton in response to the cell's requirements [5]. Microtubule assemblies determined through the concentration of free tubulins in the cytoplasm, at low concentrations the growth rate at the microtubule ends is languid and results in an increased rate of disassembly (de-polymerization) [5, 6]. Recently, especial particles have been discovered inside the microtubules that exist in different ways between cell types while the neuronal cells have the most particles [7–10]. In 1984, Burton introduces those particles that could be voided via lumen quickly through reassembly or disassembly of microtubules [11]. Proteins that destabilize or destabilized microtubules have been distinguished recently (such as stathmin family proteins and Colchicine) and the protein related to stathmin is expressed in the nervous systems which are known as SCLIP, SCG10, RB3 (and two its splice variants RB3' and RB3") [12–14]. Via electron microscopy (EM) it can be seen that each proto-filament consists of globular 4 nm subunits and it is possible for refining tubulin to assemble with a range of diameters containing between 9 and 16 protofilaments (Fig. 1).

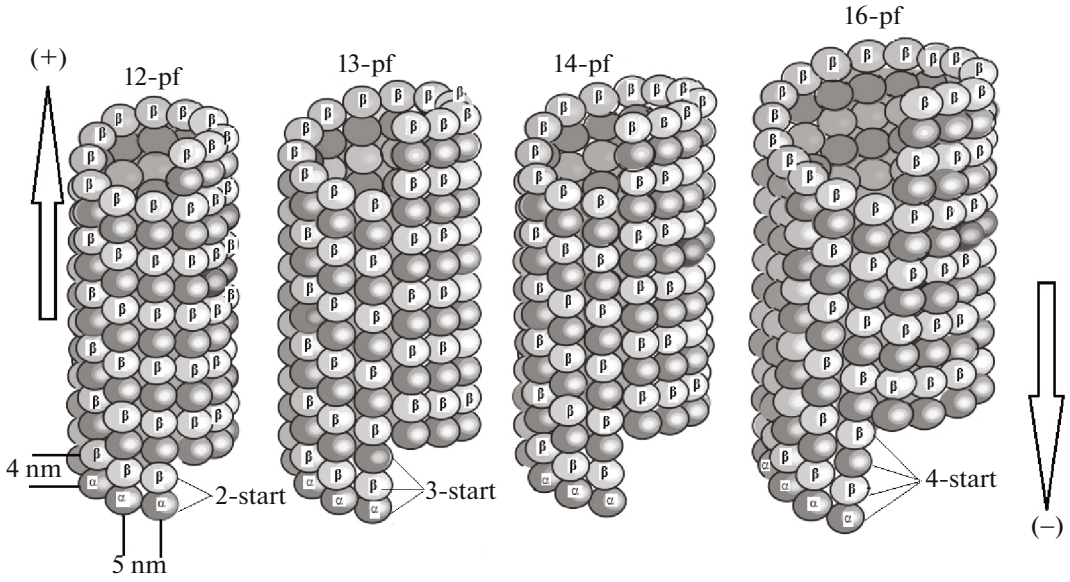


**Fig. 1.** The schematic images of various microtubules including 12–16 proto-filaments (pf).

Two major structures of αβ-tubulin are known; the first one is GDP-tubulin in straight antiparallel proto-filaments stabilized by "Taxol" and the second is the curved structure of two head to tail GDP-tubulin dimers in complex with the stathmin-like domain (RB3-SLD) (Fig. 2) [15–18]. The structures of tubulins in microtubules are related to the straight zinc-sheet structures. Monomers in adjacent proto-filaments serialize a set of shallow are helices that for 13-protofilament microtubules three shallows run in parallel. This situation causes a suitable flexibility in the bonds between adjacent hetero-dimers. The microtubules—associated motor proteins, such as dynein and kinesin can be run for long distances along a microtubule when there are 14 proto-filaments [19, 20]. In more or fewer than 14 proto-filaments, the structure might be rotated somewhat, so that the proto-filaments twisted slowly around the microtubule axis [21].

Ravelli et al. [23], exhibited some important data about the conformational changing of microtubules structures through X-ray crystallography. The monomers have a pair of spherical domains which the larger domain, contains the N-terminal half of the polypeptide. A binding site for "Taxol" is located on the second domain of αβ-tubulins, which has sufficient contact with the core helix and also on the opposite side has contact with a nucleotide base. The C-terminal end of each tubulin polypeptide makes two long helices and these residues are suitable for isoform recognition through tubulin binding proteins. As it has been shown in Fig. 3, the long coil loop of globular domain is attached in lateral contact to the proto-filament inside the microtubule. In addition, there is a common agreement that the "M-loop" of one proto-filament makes contact with the GTPase domain. In some locations the proto-filament makes a ring through bending at all of the interfaces among monomers.

Stathmin interacts with αβ-tubulin for forming a ternary complex which tubulins are able to switch between a curved structure of this complex including RB3 protein and a straight microtubule-like structure. By this study, the kinetic, potential, total and thermodynamic assemblies and dis-assemblies have been done by GTP hydrolysis in viewpoint of Monte Carlo simulation. The microtubule-associated proteins (MAPs) of tubulin-GDP proto-filament helixes have been indicated with dimer curvatures. This phenomenon indicates a proposition that the free GTP–tubulin dimers are curved similarly to tubulin rings and is driven into the straight conformation through the microtubule. Consequently, in the allosteric model, GTP binding would induce a straighter conformation pre-structured in solution for lateral interactions whereas in the lattice model αβ-tubulin adopts a microtubule incompatible and curved conformation independent of the nucleotide state.

## THEORETICAL MODE

### *Thermodynamics Approach*

The polymerization of microtubules consists of 3 steps. First, GTP-tubulin dimers ($T_{GTP}$) where can attach or detach from the tip of the microtubule. Second, GDP-tubulin dimers ($T_{GDP}$) where can only detach from the microtubule tip. Third, the $T_{GDP}$ inside the microtubule where can hydrolyses inside $T_{GDP}$. Since, the number of microtubule configurations are large therefore, $M_j$ denotes a microtubule in

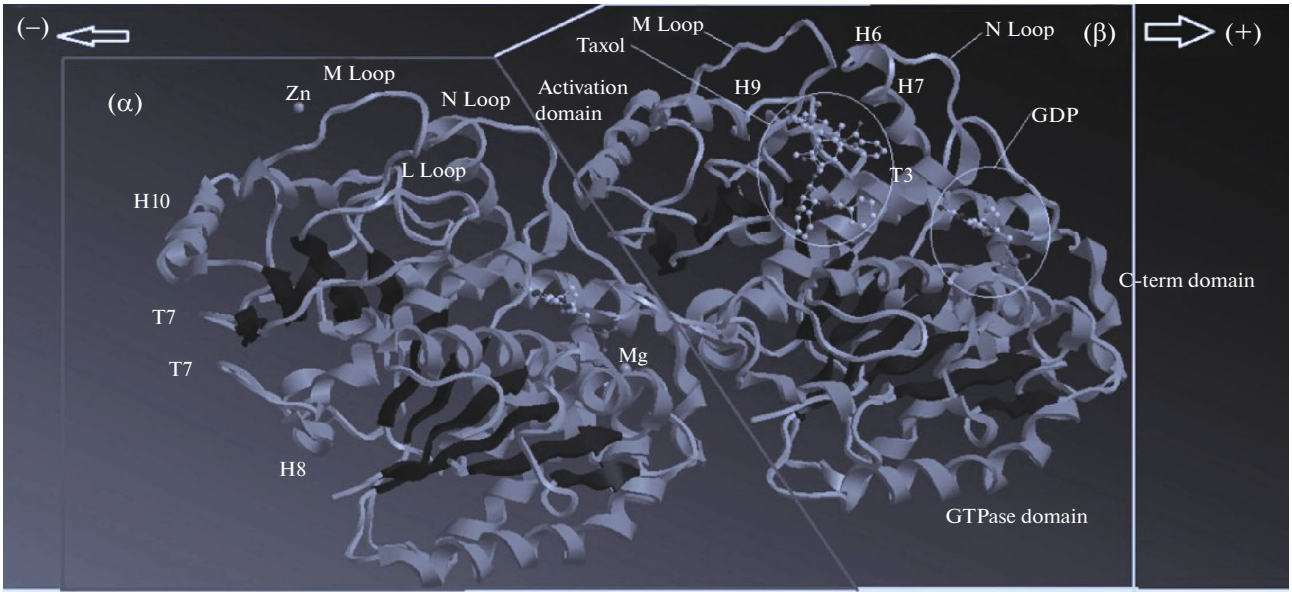


**Fig.2.** The structure designed by electron crystallography in complex with Taxol [22]. The guanosine triphosphate "GTPase" domain, the activation domains and the core helix connected to two globular domains in each monomer on the external surfaces are shown. GTP is sandwiched between α- and β-tubulin subunits of each heterodimer and of two tubulins, this pocket are occupied by the extended L-loop.

the configuration $J$. By GTP-tubulin dimer hydrolyses to a GDP-tubulin, the configuration of the microtubule changes. Those three mentioned reactions can be summarized as follows:

$$M_j + T_{GTP} \leftrightarrow M_{j'}, \tag{1}$$

$$M_j \leftrightarrow M_{j''} + T_{GDP}, \tag{2}$$

$$\begin{aligned} &M_j \leftrightarrow M_{j'''} + P_i \text{ (hydrolysis)} \\ \text{and}\quad &T_{GDP} + P_i \leftrightarrow T_{GTP} \text{ (self regulating).} \end{aligned} \tag{3}$$

That $P_i$ is an inorganic phosphate. We have added here, for completeness, the self-regulating process transforming GDP-tubulin into GTP-tubulin. The indices $J$, $J'$, $J''$, and $J'''$ are related to each other. Equation (1) is a normal system corresponding to a very large number of chemical equations. The last equation in (3) symbolizes the self-regulatory process that controls the GTP-tubulin concentration in the cell. A major configuration $M_j$ can occur on both sides of chains. We now consider a volume $V$ containing $N_j$ moles of microtubules in configuration $J$, $N_t$ moles of free GTP-tubulin dimers, $N_w$ moles of water, $N_d$ moles of free GDP-tubulin dimers and $N_p$ moles of $P_i$. A priory, we thus have $Q$ different types of microtubules, each with their own concentration $N_j$. Moreover, we know that in physiological conditions, $N_j/N_w$, $N_t/N_w$, $N_d/N_w$, and $N_P/N_w$ are very small. The Gibbs' energy of the microtubule solutions is given by

$$\begin{aligned} G(N_{j_1},\ldots N_{j_Q},\ldots N_t, N_d, N_P, N_w) &= N_w[\mu_w(T) - TS_w(T) + Pv_w(T)] \\ &+ \sum_{i=1}^{Q} N_{j_i}\left[\mu_j(T) - TS_j(T) + Pv_{j_i}(T) + RT\sum_{i=1}^{Q} N_{j_i}\ln(N_{j_i}/N_w)\right] \\ &+ N_t\left[\mu_t(T) - TS_t(T) + Pv_t(T) + RTN_t\ln\left(\frac{N_t}{N_w}\right)\right] \\ &+ N_d\left[\mu_d(T) - TS_d(T) + Pv_d(T) + RTN_d\ln\left(\frac{N_d}{N_w}\right)\right] \\ &+ N_p\left[\mu_p(T) - TS_p(T) + Pv_p(T) + RTN_p\ln\left(\frac{N_p}{N_w}\right)\right], \end{aligned} \tag{4}$$

where $\mu(T)$, $S(T)$, and $v_w(T)$ are energy, entropy, and the volume on the temperature $T$, respectively. During the association of one tubulin dimer to a microtubule $M_j$ to produce a microtubule $M_{j''}$, as in the reaction (2), the Gibbs' energy changes can be computed as

$$\begin{aligned} \Delta G_{j,j'} = G\left(\ldots N_{j'}, \ldots N_j - \frac{1}{N_a}, \ldots N_t \ldots \frac{1}{N_a}, N_d, N_p, N_w\right) - G\left(N_{j'}, \ldots N_j - \frac{1}{N_a}, \ldots N_j \ldots N_t, N_d, N_p, N_w\right). \end{aligned} \tag{5}$$

All the quantities normalized to single molecules rather than 1 mol has been computed by a Monte

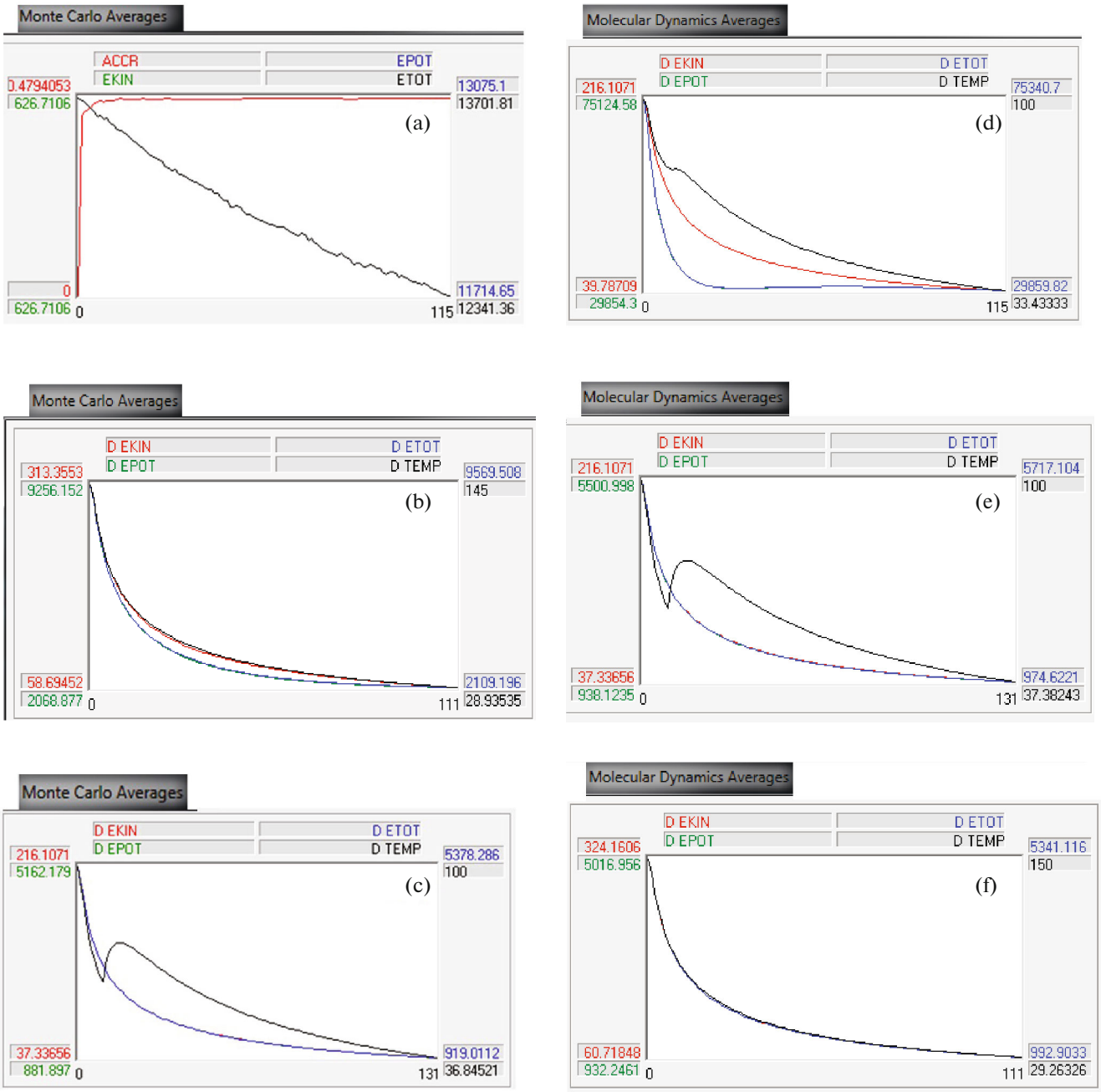


**Fig. 3.** Monte Carlo and molecular dynamic simulation of T-SLD in six stages (a–f) based on various potential and kinetic energies; red color is kinetic energy, black color is potential energy, and blue color is the total energy and *x*-axis value is the run step (number of iteration).

Carlo simulation of the chemical reaction. Using $\ln(N_j - 1/N_a)_j \cong \ln N_j$, yields:

$$\begin{aligned}\Delta G_{j,j'} &\cong (\mu_{j'} - \mu_j - \mu_t)/N_a \\ &-\frac{T(S_{j'} - S_j - S_t)}{N_a} + P(\vartheta_{j'} - \vartheta_j - \vartheta_t)/N_a \\ &+ kT\left[\ln\frac{N_{j'}}{N_w} - \ln\frac{N_j}{N_w} - \ln\frac{N_t}{N_w}\right].\end{aligned} \quad (6)$$

Equation (6) can also be used, up to a sign, for the detachment of any type of tubulin dimer.

### *MD Simulation*

**Algorithm optimization.** A suitable algorithm can be selected based on total number of atoms, system average density and system average temperature for the MD or MC simulation. By this work, the total number of atoms were set between 9600 to 14 400 thousand

while the system temperature ranges from 300 to 310 K. For atoms located around the central area, the initial condition is the thermal random motion combined with the assigned distribution of displacement. The initial conditions adopted in these simulations had T-SLD in a straight conformation normal to the surface.

We used 80–120 iteration running that lasted between 10–15 ps for each items and also each of them taken up 80% of these values for relaxation time and 20% for stabilization of the various resultant conformations that were then statistically analyzed. These simulations were run on a personal computer with a 4 GHz Pentium dual CPU and 2.0 GB DDR RAM for run steps among 80–120 for MD and MC simulation. The model parameters used for the numerical evaluation, First, we have used the geometrical dimensions of the tubulin dimer as: $H = 8$ nm, $W = 6$ nm. Then, we assumed that approximately 2/3 of the net average charge of tubulin is exposed on the outer surface The empirical estimate of the relative dielectric constant $\varepsilon_r$ based on Mallik works which, is linearly approximated by: $\varepsilon_r(d) = 1 + \frac{79d}{1.7}$, $d \le 1.7$ [24].

Before an algorithm comes to realization, its accuracy and efficiency first have to be verified. The accuracy of MD simulation results such as displacement and velocity are identical and thus do not need to be inspected. However, only the theoretical prediction for the efficiency optimization has been provided so far, and the numerical validation through a real case is still required.

**Potential interaction among particles.** There are several methods to compute the minimum energy for interaction among the particles but most widely used methods are steepest descent and conjugate gradient that utilizes the gradient of the potential energy surface. It directly relates to the forces in the molecular mechanical description of molecular systems, to guide a search path toward the nearest energy minimum. Molecular mechanics force fields are the basic of bio-macromolecular simulations, being used to compute the potential energy of a system of particles.

Force fields provide information about the potential energy interactions among particles in microtubule system that are explained via Lennard-Jones potentials as follows:

$$V_{\mathrm{LJ}}(r_{ij}) = 4\varepsilon_{ij}\left\{\left[\left(\frac{\sigma_{ij}}{r_{ij}}\right)^{12} - \left(\frac{\sigma_{ij}}{r_{ij}}\right)^{6}\right]\right\}, \quad r < R_C, \qquad (7)$$

$R_C$ is a cutoff distance around 12 Å for T-SLD. Absolute value of inter-atomic potential or inter-atomic force decays very fast to zero when the inter-atomic distance gets larger than several times the equilibrium distance, a cut-off radius, $R_C$ is usually defined so that the neighboring atoms outside this radius will be ignored. Using this cut-off radius, the interaction among atoms is actually reduced to a short-range type. It is worth mentioning that Van der Waals interaction terms, described by a Lennard-Jones [25] potential function, include only dispersion or London interactions between transient dipoles, while Keesom interactions (between permanent dipoles) and Debye (induced dipole) interactions are included in the electrostatic (Coulomb) term, without explicit development into charge distribution momenta. In addition the Lorentz–Berthelot rules have been applied for the inter forces among MTs and tubulins–stathmin-like domain complex (T-SLD) as follows:

$$\sigma_{ij} = 0.5(\sigma_i + \sigma_j) \quad \text{and} \quad \varepsilon_{ij} = \sqrt{\varepsilon_i}\sqrt{\varepsilon_j}. \qquad (8)$$

the non-bonded and bonded data including van der Waals of related force fields are listed in Tables 1 and 2. The total energies of the model systems are a total of several partial energies as follows:

$$E_{\mathrm{system}} = E_{\mathrm{bond}} + E_{\mathrm{angle}} + E_{\mathrm{torsion}} + E_{\mathrm{over}} + E_{\mathrm{vdW}} + E_{\mathrm{Coulomb}}, \qquad (9)$$

where $E_{\mathrm{bond}}$ and $E_{\mathrm{angle}} + E_{\mathrm{torsion}}$ are bond formation and angle (both strain and torsional) energies, respectively; $E_{\mathrm{over}}$ is associated with valence and torsional angles, respectively that prevents the over-coordination of the atoms; $E_{\mathrm{vdW}} + E_{\mathrm{Coulomb}}$ are the dispersive and electrostatic energies contribution between all atoms, respectively. The TIP3 model uses a total of the three sites for the electrostatic interactions. The partial positive charges on the hydrogen atoms are exactly balanced by an appropriate negative charge located on the oxygen atom. The OPLS model is a modified form of TIPS that has parameters fitted to liquid state properties, and so is more suitable for studies of liquids. The model works well for a variety of alcohols, amines, aliphatic and aromatic hydrocarbons, sulfur compounds, ether, amino acids, and nucleic acid bases.

The OPLS Lennard-Jones parameters for nucleic acid bases are included in Table 3. There are multiple force fields available, and selection of the most adequate force field in studies bio-macromolecular simulations including AMBER [25], and CHARMM in which an empirical energy function that contains terms of both internal and external interactions was used [26].

**Simulated model.** A model of tubulins–stathmin-like domain complex with a radius of 20 μm and a height of 0.4 μm for a volume of approximately 900 $\mu m^3$ has been simulated where MTs are nucleated from a defined number of sites located in the center of a cylinder (Table 4). It is notable, one state with index $i$, is connected to other $N$ states, indexed by $j = 1, \ldots, N$, by transitions that happens with rates $\tau_{ij}$ (from $i$ to $j$). At each iteration of the algorithm, one of the $N$ transitions is randomly chosen (with the right probability), and the *time step* is cleverly calculated using a

**Table 1.** Non-bonded interaction parameters in terms of $E_{\text{Van der Waals}} + E_{\text{Coulomb}}$

$$V_{LJ}(r_{ij}) = 4\varepsilon_{ij}\left\{\left[\left(\frac{\sigma_{ij}}{r_{ij}}\right)^{12} - \left(\frac{\sigma_{ij}}{r_{ij}}\right)^{6}\right]\right\}, r < R_C$$

| atom type | mass, g/mol | σ, nm | ε, kcal/mol |
|---|---|---|---|
| $CH_2$ | 14.03 | 0.393 | 0.081 |
| C=O | 28.05 | 0.444 | 0.019 |
| O–H | 17.08 | 0.241 | 0.034 |
| C–O | 28.07 | 0.315 | 0.010 |
| C–C | 24.03 | 0.133 | 0.082 |
| N–C | 26.01 | 0.366 | 0.065 |
| P–O | 33.4 | 0.448 | 0.088 |

random number $u$ in (0, 1](0, 1] by $\Delta t = \frac{\ln(1/u)}{R}$, where $R$ is the sum of all the rates of the transitions leaving from state $i$. In this way $\Delta t$ is exponentially distributed with mean $1/R$. Since the T-SLD surface is complicated we use a dense grid that models its charge distribution. The outer surface can be characterized as mainly negative with a few small positive pockets. The computation of the interaction between the stathmin and the dimer's surface is highly intensive if done for each update of the position. By using 2 Å resolution, the number of grid points is $(8/0.2) \times (6/0.2) = 1200$, assuming a $6 \times 8$ nm$^2$ surface area. But we used several of bead models (including 8, 10, and 12) then the number of point-to-point interactions becomes 9600, 12000, and 14400 numbers, respectively. Although a reasonable number of updates are $10^5$ to $10^6$, so this type of interaction becomes a serious bottleneck. For overcoming this problem, we assume that the surface is static and evaluate the field it exerts in a box of $(6 \times 8 \times 6)$ nm$^3$ volume whose base is the surface.

In Table 4, the input distributions can be either *continuous*, where the randomly generated value can take any value under the distribution (for example a normal distribution) or *discrete*, where probabilities are attached to two or more distinct scenarios. To set up the Monte Carlo simulation. Options dialog box allows us to set up the Monte Carlo simulation parameters. And we are able to run a constant temperature simulation with various steps. For some systems, it may be useful to add optional heat and cool phases. Set the run steps to 100 and also set the heat and cool steps and also the maximum step size (max delta) around 0.05–0.1 Å are the most condition of our Monte Carlo simulation. The Monte Carlo averages setup is identical to molecular dynamics averages setup. There is an additional parameter that you can monitor in Monte Carlo: the acceptance ratio. The acceptance ratio is a running average of the ratio of the number of accepted moves to attempted moves. Optimal values are close to 0.5. Varying the step size can have a large effect on the acceptance ratio.

### *Simulation of Tubulins–Stathmin-Like Domain Complex (T-SLD)*

T-SLD simulation is done to replicate the experimental conditions, so several parameters for the different physical conditions are considered (such as pressure, temperature). In general the protein simulation is done in canonical ensemble (*NVT*), particularly the initial equilibration steps, or isothermal-isobaric (*NPT*) ensemble. The simple structure emulators the basic area of a generic cell binding for the minimum slip where MTs and tubulins–stathmin-like domain complex (T-SLD) are dynamically measured. The concentrations of total tubulins were basically set between 30–35 μM [27, 28]. For increasing the efficiency of simulations, the number of nucleation site were modeled to 400, which also collected the maximum number of T-SLD. Additional presumptions have been considered as (1) tubulins–complete T-SLD

**Table 2.** Parameters of bonded interactions of the atomistic force field

$$\left\{\left[V_b(r_{ij}) = \sum_{\text{bonds}} k_{ij}^b (r_{ij} - b_{ij})^2\right]\right\} + \left\{\left[V_\beta(\theta_{ijk}) = 0.5 \sum_{\text{angle}} k_{ijk}^\theta (\theta_{ijk} - \theta_{ijk}^0)^2\right]\right\} + \{[V(\varphi_{ijkl})k_\varphi(1 + \cos(n\varphi - \delta)$$

| bond | $b$, Å | $k^b$, kcal/(mol Å$^2$) | angle | $\theta_{ijk}^0$ | $k_{ijk}^\theta$, $\frac{\text{kcal}}{\text{mol}} \times \text{rad}^2$ | dihedral $\varphi_{ijkl}$ | $k_\varphi$, kcal/mol | $n$ | δ |
|---|---|---|---|---|---|---|---|---|---|
| C–H | 1.11 | 335 | C–O–C | 117.5 | 53.5 | C–C–C–O | 0.35 | 1 | 0.00 |
| C=O | 1.21 | 330 | C–C–C | 121.1 | 65.5 | H–C–C–C | 0.40 | 3 | 180.0 |
| O–H | 1.09 | 350 | O–C–O | 118.4 | 45.4 | O–C–C–H | 0.24 | 2 | 0.00 |
| C–O | 1.41 | 240 | C–C–H | 111.1 | 46.4 | C–O–C–H | 0.43 | 2 | 0.00 |
| C=C | 1.34 | 355 | O–C–H | 109.2 | 44.5 | O–C–C–O | 0.61 | 3 | 0.00 |
| P–O | 1.44 | 370 | P–O–C | 110.4 | 49.5 | P–O–C–C | 0.75 | 3 | 180.0 |

**Table 3.** OPLS Lennard-Jones parameters for nucleic acid bases

| Atom | σ, Å | ε, kcal/mol |
|---|---|---|
| O | 2.85 | 0.215 |
| N | 3,41 | 0.175 |
| C in C=O | 2.85 | 0.120 |
| P | 3.65 | 0.135 |
| H(N) | 0.0 | 0.0 |
| H(C) | 2.15 | 0.09 |
| H(O) | 1.85 | 0.11 |

depolymerization immediately opens up that nucleation site for a new nucleation event [28, 29]; (2) all T-SLD remain associated with their nucleation site until they completely depolymerize and do not bend during confliction with the cell margin; (3) T-SLD de-stabilization is dependent on free tubulin concentration; (4) any T-SLD destabilization reaching the cell boundary undergoes a catastrophe. Simulations with time step = 1 s obeyed the general sequences as: (1) available places are checked for nucleation based on the given probability; (2) T-SLD with a velocity determined by free tubulin concentration; (3) stabilization/destabilization of T-SLD can remain in a catastrophe, there by switching to a shortening state. T-SLD that achieves the cell boundary will move to a shortening state; (4) shortening T-SLD can continue to shorten or undergo a liberation phenomenon. Output from this modeling are including, number and lengths, free tubulin concentration, the length of a single T-SLD during the simulation and thermodynamic parameters. Common data and values applied for simulating the interphase T-SLD array. Nucleation rate were estimated based on previous work from the centrosome [28, 29] divided by the 450–500 potential sections. Total tubulin concentrations were calculated as described previously [27, 28]. There are multiple steps involved in simulation and Fig. 3 shows some of the most important ones. MD simulation starts with the knowledge of the potential energy of the system with respect to its position coordinates. The first derivative of the potential function to the position coordinates helps to compute the force acting on individual atoms of the system. The essential steps involved in the MD simulations of proteins are as follows. The clear measure constants, $K_{on}$ and $K_{off}$ were applied for calculating assembling and deassembling measuring as a function of free tubulin concentration. The initial parameters were tested based on interphase LLCPK1 cells [28–30]. In addition, all information about geometeries, energies and end dynamic instability based on Monte Carlo and molecur dynamic methods are listed in Tables 2–5 and Fig. 3.

As shown in Fig. 3a, the distributions of T-SLD lengths forms a tightly exponential, where T-SLD ends is limited to an area near the edges, based on defined by the cell radius. The length of one molecule T-SLD is exhibited in Fig. 3b. Consistent with the distribution of all T-SLD ends, the end of this single T-SLD spends maximum of its time close the cell boundary. Figure 3c exhibits a simulation run for fewer steps to show the early steps in T-SLD assembly for a single T-SLD. Slower speed, as tubulins are combined into T-SLD, were trivial through changes in the slope on the first growth section. Medium T-SLD quickly reached about 20 μm (Fig. 3d).

The total number of T-SLD increased for 4500 microtubules via around 4000 s. We applied the simulations of free tubulin concentration in a steady state amounts through Fig. 3e and the standard deviations of those values also in Fig. 3f.

### *Stathmin and Microtubule Dynamics*

Microtubules exist in a situation of continuous transition between two phases of polymerization and depolymerization which is based on dynamic instabilities with a stochastic mechanism which this phenomenon is known as catastrophe (Fig. 4). In intermediate struc-

**Table 4.** Common simulation parameters of both Monte Carlo simulation (a, b, and c) and molecular dynamic simulation (d, e, and f)

| Simulation temperatures | Random seeds | Run step (number of iteration) | Time step, ps $\Delta t = \frac{\ln(1/u)}{R}$ | Maximum step size or max delta, Å | Run time, ps | Numbers of atoms | Various steps |
|---|---|---|---|---|---|---|---|
| Monte Carlo simulation | | | | | | | |
| 300 | 18077 | 100 | 0.05 | 0.05 | 10.0 | 14400 | a |
| 305 | 24000 | 90 | 0.06 | 0.04 | 15.0 | 12000 | b |
| 310 | 22600 | 80 | 0.07 | 0.06 | 12.0 | 9600 | c |
| Molecular dynamic simulation | | | | | | | |
| 300 | 20000 | 120 | 0.08 | 0.07 | 14.0 | 14400 | d |
| 305 | 25000 | 100 | 0.09 | 0.05 | 9.0 | 12000 | e |
| 310 | 30000 | 110 | 0.1 | 0.05 | 11.0 | 9600 | f |

**Table 5.** Potential ($E_p$) and kinetic ($E_k$) energies (kcal/mol) steps a–f for Taxol with the stathmin-like domain interaction (T-SLD), $T_s$ is simulation temperature

| $T_s$, K | $E_p$ | $E_k$ | $E_{total}$ | Step |
|---|---|---|---|---|
| Monte Carlo simulation | | | | |
| 300 | 13074.1 | 626.7 | 13700.8 | a |
| 305 | 75342.7 | 216.1 | 77558.8 | b |
| 310 | 9569.5 | 314.3 | 9883.8 | c |
| Molecular dynamic simulation | | | | |
| 300 | 5717.1 | 217.1 | 5934.2 | d |
| 305 | 5379.2 | 266.1 | 5645.3 | e |
| 310 | 5343.1 | 324.1 | 5667.2 | f |

ture, microtubule is long and stable with its dynamic relatively slow. Belmont [31] supposed a model to exhibited stathmin exerts effects via increasing the rate of catastrophe and consequently an explanation in which the microtubule-depolymerized. The mechanism is based on stathmin binds two un-polymerized tubulins in ternary stathmin–tubulin complexes (Fig. 4). The tubulin-sequestering activities of the stathmin prevent any growth of microtubule through tubulin polymerization. The catastrophe-promoting activities are confirmed for occurring at the ends of polymerization and also exhibit how does stathmin binds tubulin heterodimers at the microtubule ends for increasing catastrophe via a GTP hydrolysis-dependent mechanism structure of the complex of tubulin and also the stathmin-like domain (SLD) of RB3. The tubulins subunits in the complex are associated head-to-tail in a curved conformation. The same group recently extended these observations by showing that the curved complex is capped by the amino-terminal region of the SLD domain. This prevents the incorporation of the complex into polymerized microtubules. These investigations exhibit that stathmin are able to bind both polymerized and un-polymerized tubulins and is able to exclude the polymerization towards a stable microtubule.

*Estimation of Kinetic and Free Energies*

In the kinetic reaction the rate constant of association and dissociation are as $K_a$ and $K_d$, respectively. The free energy for the association reaction is $\Delta G_a = -RT \ln K$ with the relation of $K = \frac{K_a}{K_d}$. For simplicity it can be supposed that the $K_a$, is equal for all sites, therefore a fixed-geometry binding site is applied due to highest affinity of tubulin–GTP interaction comprising to the isolated site. The $K = \frac{K_a}{K_d}$ values can be calculated using estimated free energies values of individual bonds with definition of association and dissociation sites.

The affinities of the tubulins dimer for a microtubule end then depends upon the number of contacts formed. The free energies for the binding of one molecule of tubulin-GTP at the especial sites may be obtained as the sum of the free energies for individual subunit–subunit interactions between tubulin monomers. The binding of a molecule of tubulin-GTP to a typical site may be formally regarded as involving free energy terms (Fig. 1).

## RESULT AND DISCUSSION

Monte Carlo simulation has been applied to study dynamic instability of the microtubule length of our model based on the papers [32]. In this method one-dimensional microtubule is fixed at one of the two and simulated while the opposite end is allowed for growing in random situation. In this model at each step one tubulin has been added to the length for growing microtubule length. Computationally this can be done through generating a uniform random number between 0 and 1. Comparing the data for dynamical instabilities among parameter sets exhibited that rates of elongation and shortening varies to the small degrees. For testing how the differences data among the parameters contribute to the overall microtubule arrays, it can be simulated with those parameters from

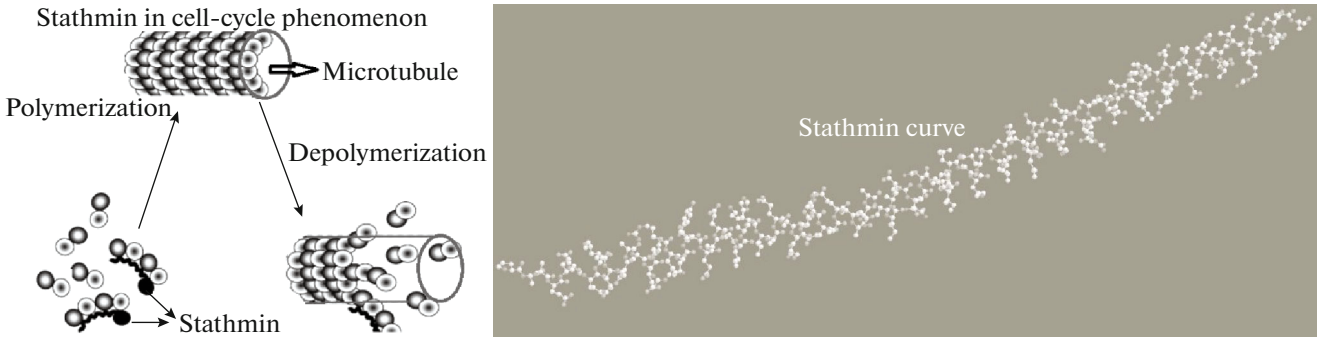


**Fig. 4.** Model for the role of stathmin in the regulation of microtubule dynamics during polymerization and de-polymerization in a cell cycle phenomenon.

one set and basically switched that data at a time to that from the other set. It might be considered the effect of stathmin concentration gradient for formation of microtubule length. So the model of quasi-one-dimensional constriction of microtubules has been selected. In this model, the microtubule formation switches among assemblies states and dis-assemblies with the random variables of Monte Carlo approach.

A transition frequency $f_t$ has been defined for assembly states to disassembly situation of catastrophe and $f_{t-1}$ has been defined from dis-assemblies to assembly. Based on several parameters like formation and constriction velocities, tubulin concentration have to describe through the simplest stochastic model of field equations based on Leibler work to study this matter using Monte Carlo simulation of microtubule length [33]. This model consist of a cell including free αβ-tubulins and stathmin which are distributed uniformly. The accessibility of free αβ-tubulins in the cell pertains on the concentration of the stathmin due to each stathmin binds to two αβ-tubulins towards threemeric structure.

If the corresponding changes in conformation also elevate the rate of GTP hydrolysis at remote sites in the stabilizing cap, then EB's preference for a "twisted and compacted" conformation at one site has the potential to accelerate GTP hydrolysis elsewhere. We speculate that whether acting through GTPase activity or not, lattice-propagated modulation of αβ-tubulin conformation and biochemistry, and the threshold-dependent effects that may accompany this long-range coupling, will be important for understanding fundamental mechanisms of microtubule dynamics in general [34–37].

However, these situations of stathmin proteins are weakened around mitotic chromosome because of stathmin's phosphorylation. It might be supposed that from the centrioles towards the chromatin position, the activities of stathmin are uniform till a certain distance, and then there is a gradual inhibition of stathmin activities which are approximately zero at the chromatin. As a result, one finds a gradient of stathmin–tubulin interaction as one move towards the chromatin as reported by Niethmmer experimentally [38].

At any immediate of time microtubules end are in one of the two situation, length and or simplifying. In this simulation a regular steps of time $t$ it might be possible for adding or subtracting one tubulin length for growing or simplifying microtubules elongation. If $f_t$ and $f_{t-1}$ are the transitions frequencies for catastrophe and rescue, respectively then the normalized equations of those frequencies can be written as: $f_{\text{catastrophe}} = \dfrac{f_t}{f_t + f_{t-1}}$ and $f_{\text{rescue}} = \dfrac{f_{t-1}}{f_t + f_{t-1}}$. The microtubule elongation at a especially immediate of time will be in length situation or simplifying states if the random numbers are less than the normalized transition frequencies for catastrophe, $f_t$ or rescue, $f_{t-1}$. Obviously, it must be supposed the transitions to be instantaneous and with a definition of critical length, $L_{\text{critical}}$, $f_{\text{catastrophe}}$, and $f_{\text{rescue}}$ (with an exponential function) are constant. In this position the velocities of growth is $V_{\text{growth}}$ and for shrinkage $V_{\text{shrinkage}}$ for the microtubules (Table 6). These data are reasonable and also confirm the experimental information [38, 39].

**Table 6.** Kinetic and thermodynamic parameters for Taxol with the stathmin-like domain interaction (T-SLD)

| System | $V_{\text{growth}}$, μm s$^{-1}$ | $V_{\text{shrinkage}}$, μm s$^{-1}$ | $K_a$, s$^{-1}$ | $K_d$, s$^{-1}$ | $k$ | $\Delta G$ |
|---|---|---|---|---|---|---|
| Monte Carlo simulation | | | | | | |
| A | 0.224 | 0.154 | 0.054 | 0.066 | 0.83 | −495.5 |
| B | 0.199 | 0.166 | 0.045 | 0.077 | 0.58 | −131.5 |
| C | 0.213 | 0.188 | 0.064 | 0.081 | 0.79 | −587.9 |
| Molecular dynamic simulation | | | | | | |
| D | 0.191 | 0.149 | 0.057 | 0.066 | 0.86 | −376.1 |
| E | 0.189 | 0.155 | 0.067 | 0.065 | 0.96 | −357.8 |
| F | 0.178 | 0.167 | 0.077 | 0.065 | 0.88 | −453.9 |

## CONCLUSIONS

Microtubules are demonstrated as straight macromolecules consist of the linear chains of tubulin subunits in the length without any incorporating molecular details of tubulin dimers, protofilament or other structures. It has been calculated a correct dimension around $10^{-6}$ m of microtubules length consist of around 1650 tubulin dimers. Microtubule growth rate is related to the soluble tubulin dimer concentration and for all results shown here, simulation of any single condition was run 5–10 times. MD simulations can help us to visualize and understand conformational changes at an atomic level when combined with visualization software which can display the structural parameters of interest in a time dependent way.

## CONFLICT OF INTEREST

The authors declare that they have no conflicts of interest.

## REFERENCES

1. D. Ringhoff and L. Cassimeris, Mol. Biol Cell. **20**, 3451 (2009). https://doi.org/10.1091/mbc.E09-02-0140
2. M. J. Clément, I. Jourdain, S. Lachkar, et al., Biochemistry **44** (2005). https://doi.org/10.1021/bi0512492

3. B. K. Garvalov, B. Zuber, C. B. Marquis, et al., J. Cell Biol. **174**, 759 (2006).
4. G. I. Brouhard and L. M. Rice, J. Cell Biol. **207**, 323 (2014). https://doi.org/10.1083/jcb.201407095
5. A. Akhmanova and M. O. Steinmetz, Nat. Rev. Mol. Cell Biol. **16**, 711 (2015). https://doi.org/10.1038/nrm4084
6. Y. Chen and W. O. Hancock, Nat. Commun. **6**, 8160 (2015). https://doi.org/10.1038/ncomms9160
7. S. Sahu, S. Ghosh, B. Ghosh, et al., Biosens. Bioelectron. **47**, 141 (2013).
8. A. Guesdon, F. Bazile, R. M. Buey, et al., Nat. Cell Biol. **18**, 1102 (2016). https://doi.org/10.1038/ncb3412
9. K. K. Gupta, E. O. Alberico, I. S. Näthke, and H. V. Goodson, Bio Essays **36**, 818 (2014). https://doi.org/10.1002/bies.201400029
10. P. K. Hepler, Plant Physiol. **170**, 3 (2016). https://doi.org/10.1104/pp.15.0150626722019
11. P. R. Burton, J. Cell. Biol. **99**, 520 (1984).
12. D. C. Rowlands, A. Williams, N. A. Jones, et al., Lab Invest. **72**, 100 (1995).
13. S. Ozon, A. Maucuer, and A. Sobel, Eur. J. Biochem. **248**, 794 (1997).
14. E. Charbaut, P. A. Curmi, S. Ozon, et al., J. Biol. Chem. **276**, 16146 (2001).
15. S. M. Hanash, J. R. Strahler, R. Kuick, et al., J. Biol. Chem. **263**, 12813 (1988).
16. P. A. Curmi, C. Nogues, S. Lachkar, et al., Br. J. Cancer **82**, 142 (2000).
17. D. K. Price, J. R. Ball, Z. Bahrani-Mostafavi, et al., Cell **84**, 623 (1996).
18. L. D. Belmont and T. J. Mitchison, Cell **84**, 623–631 (1996). https://doi.org/10.1016/s0092-8674(00)81037-5.
19. N. Hirokawa, Science (Washington, DC, U. S.) **279**, 519 (1998).
20. R. D. Vale, Cell **112**, 467 (2003).
21. R. H. Wade, D. Chrétien, and. D. Job, J. Mol. Biol. **212**, 775 (1990).
22. E. Nogales, S. Wolf, and K. H. Downing, Nature (London, U.K.) **391**, 199 (1998).
23. R. B. G. Ravelli, B. Gigant, P. A. Curmi, et al., Nature (London, U.K.) **428**, 198 (2004).
24. B. Mallik, A. Masunov, and T. Lazaridis, J. Comput. Chem. **23**, 1090 (2002).
25. Y. Duan, C. Wu, S. Chowdhury, et al., J. Comput. Chem. **24**, 1999 (2003).
26. B. R. Brooks, C. L. Brooks, A. D. MacKerell, Jr., et al., J. Comput. Chem. **30**, 1545 (2009).
27. B. T. Castle, S. McCubbin, L. S. Prahl, et al., Mol. Biol. Cell. **28**, 1238 (2017). https://doi.org/10.1091/mbc.E16-08-056728298489
28. M. Piehl, U. S. Tulu, P. Wadsworth, and L. Cassimeris, Proc. Natl. Acad. Sci. U. S. A. **101**, 1584 (2004).
29. S. S. Andersen, A. J. Ashford, R. Tournebize, et al., Nature (London, U.K.) **389**, 640 (1997).
30. N. M. Rusan, U. S. Tulu, C. Fagerstrom, and P. Wadsworth, J. Cell. Biol. **158**, 997 (2002). https://doi.org/10.1083/jcb.20020410912235119
31. L. D. Belmont and T. J. Mitchison, Cell **84**, 623 (1996).
32. D. J. Odde and H. M. Buettner, Ann. Biol. Eng. **23**, 268 (1995).
33. S. Leibler and M. Dogterom, Phys. Rev. Lett. **70**, 1347 (1993).
34. F. Mollaamin, F. Kandemirli, and M. Monajjemi, Biointerface Res. Appl. Chem. **12**, 3780 (2022). https://doi.org/10.33263/BRIAC123.37803789
35. M. A. Moulaee, M. Monajjemi, J. Mehrzad, et al., Biointerface Res. Appl. Chem. **12**, 1428 (2022). https://doi.org/10.33263/BRIAC122.14281436
36. M. Monajjemi, F. Kandemirli, H. Sakhaeinia, and F. Mollaamin, Biointerface Res. Appl. Chem. **12**, 2646 (2022). https://doi.org/10.33263/BRIAC122.26462659
37. M. A. Moulaee, M. Monajjemi, J. Mehrzad, et al., Biointerface Res. Appl. Chem. **11**, 9501 (2021). https://doi.org/10.33263/BRIAC112.95019512
38. P. Niethmmer, P. Bastiaens, and E. Karsenti, Science (Washington, DC, U. S.) **303**, 1862 (2004).
39. P. N. Zakharov, V. Gudimchuk, A. Voevodin, et al., Biophys. J. **109**, 2574 (2015). https://doi.org/10.1016/j.bpj.2015.10.048